Research article
Food Eng. Prog. 2025;29(4):239-247
pISSN: 1226-4768, eISSN: 2288-1247
https://doi.org/10.13050/foodengprog.2025.29.4.239

산업식품공학
Food Engineering Progress

Effects of aging on the physicochemical, mechanical, and gas barrier properties of edible shellac–cellulose nanofiber composite films with different blending ratios

Dong Hoon Kim[1], Yohan Song[1], Gunhyung Park[1], Huin Lee[1], Hee Chung[2], Hyo Jin Kim[1,2] and Donghwa Chung[1,2,*]

[1]Food Technology Major, Graduate School of International Agricultural Technology, Seoul National University, Pyeongchang 25354, Korea
[2]Institute of Food Industrialization, Institutes of Green Bio Science and Technology, Seoul National University, Pyeongchang 25354, Korea

Abstract

In this study, we investigated the effects of aging treatment on the physicochemical, mechanical, and barrier properties of edible composite films prepared from shellac (Sh) and cellulose nanofiber (CNF) with different blending ratios. Sh–CNF films (0%, 20%, and 50% CNF) were fabricated and subjected to aging for 7 days at 40°C and 53% relative humidity. Film thickness was found to decline with both CNF incorporation and aging, whereas there were corresponding increases in opacity, particularly in Sh-rich films. In addition, the moisture content and water solubility of films declined at higher CNF ratios, and aging contributed to further reductions in moisture content, although had no significant effects on water solubility. Color analysis revealed that aging promoted the yellowing of pure Sh films, whereas the addition of CNF mitigated these changes. The findings of mechanical analysis revealed that CNF enhanced tensile strength, yield stress, Young's modulus, and work of break, although reduced elongation at break. Aging contributed to further enhancements of strength and stiffness, along with a reduction in flexibility, although the magnitude of change diminished at higher CNF contents. Furthermore, the findings of gas barrier analysis indicated that CNF was associated with reductions in oxygen permeability, although promoted increases in water vapor permeability, with aging having the opposite effects. Collectively, these findings revealed that the functional properties of Sh–CNF films can be tailored via controlled aging and blending, thereby highlighting the potential utility of these films as edible packaging materials.

Keywords: Shellac, Cellulose nanofiber, Edible film, Aging, Gas barrier

Introduction

Shellac (Sh) is a water-insoluble, low-molar-mass natural polyester resin secreted by the insect *Laccifer lacca*. Its primary composition is an oxyacid polyester formed through esterification of aleuritic acids and cyclic terpene acids (Yuan et al., 2021; Kim et al., 2024). Classified as generally recognized as safe (GRAS), Sh exhibits excellent film-forming ability and gas barrier properties, which has led to its widespread use as a coating and film-forming agent in the food and pharmaceutical industries (Luangtana-anan et al., 2007; Yuan et al., 2021; Thombare et al., 2022; Kumar et al., 2023). However, Sh films suffer from low tensile strength and increased brittleness during drying and aging, which restrict their practical applications (Soradech et al., 2013; Chen et al., 2024).

This aging phenomenon is primarily attributed to esterification between -COOH and -OH groups of Sh molecules under the influence of heat, light, oxygen, metal ions, and pH, which promotes self-polymerization or crosslinking (Farag & Leopold, 2009; Bar & Bianco-Peled, 2021; Chen et al., 2024). Notably, Coelho et al. (2012) reported that crosslinking during Sh photoaging

Received: Sep 26, 2025 / Revised: Nov 10, 2025 / Accepted: Nov 14, 2025
Corresponding author: Donghwa Chung, Food Technology Major, Graduate School of International Agricultural Technology, Seoul National University, Pyeongchang 25354, Korea
E-mail: dchung@snu.ac.kr

results from hydrogen bonding involving aleuritic acid generated through de-esterification. To mitigate the associated increase in brittleness, various approaches have been investigated, including (1) blending Sh with other biopolymers such as gelatin, pectin, starch, or cellulose derivatives; (2) incorporating plasticizers such as polyethylene glycol, diethyl phthalate, triacetin, triethyl citrate, or oleic acid; (3) introducing salts such as calcium phosphate; or (4) applying chemical grafting with acrylic monomers, all of which improve molecular flexibility and hinder self-polymerization (Luangtana-anan et al., 2007; Soradech et al., 2013; Ahuja & Rastogi, 2024; Chen et al., 2024; Wang et al., 2025).

Cellulose Nanofiber (CNF), a nanoscale material derived from cellulose, typically has diameters of 5–30 nm and micrometer-scale lengths, with a high aspect ratio and crystallinity of up to ~65% (Poulose et al., 2022; Guivier et al., 2024). CNF films exhibit excellent tensile strength, oxygen barrier capacity, and thermal stability, in addition to being biodegradable, making them highly attractive as sustainable food packaging materials (Sharma et al., 2019; Pakharenko et al., 2021; Basumatary et al., 2022). Nonetheless, CNF is characterized by poor film-forming ability, high moisture sensitivity-which reduces its barrier properties under humid conditions-and low flexibility. To overcome these limitations, extensive studies have explored blending CNF with natural polymers such as Sh, corn starch, chitosan, polylactide, sodium caseinate, soy protein, gelatin, and mucilage, as well as incorporating plasticizers such as glycerol (Yu et al., 2017; Alves et al., 2019; Pirozzi et al., 2021; Guivier et al., 2024; Kim et al., 2024).

Recently, Kim et al. (2024) demonstrated that Sh-CNF composite films can integrate the plasticity and transparency of Sh with the mechanical strength of CNF, enabling the design of customized edible films through compositional tuning. However, Sh-based films remain susceptible to property changes during aging. Therefore, this study aimed to fabricate Sh-CNF composite films with varying blending ratios and to systematically investigate the effects of Sh aging (40℃, 53% relative humidity, 7 days) on their physicochemical, mechanical, and gas barrier properties.

Materials and Methods

Materials

CNF derived from oat was kindly provided by the Korea Textile Machinery Convergence Research Institute (Gyeongsan, Korea). The preparation procedure is briefly described as follows. Oat powder (VITACEL® Oat Fiber HF 600-30, J. Rettenmaier & Söhne GmbH & Co, Rosenberg, Germany) was suspended in distilled water and hydrolyzed using a commercial cellulase (Celluclast® BG, Novozymes A/S, Bagsværd, Denmark). The hydrolyzed suspension was then subjected to high-pressure homogenization (NH 4000, Ilshin Autoclave Co., Ltd., Daejeon, Korea) to obtain a 1.5% (w/w) CNF suspension. Edible dewaxed bleached Sh powder was purchased from Shellac Korea (Busan, Korea). $NaHCO_3$ was obtained from Junsei Chemical Co. Ltd. (Tokyo, Japan), and NaCl and glycerol were obtained from Daejung Chemicals and Metals (Siheung, Korea). $CaCl_2$, $Mg(NO_3)_2$, and NaBr were purchased from Samchun Pure Chemical Co., Ltd. (Seoul, Korea).

Preparation of Sh-CNF dispersions and composite films

Sh powder was suspended in 0.3 M $NaHCO_3$ aqueous solution at a concentration of 10% (w/w). The mixture was homogenized using a high-speed homogenizer (T25 digital Ultra-Turrax, IKA, Königswinter, Germany) at 10,000 rpm for 3 min, followed by stirring at 60℃ and 500 rpm for 10 min to prepare the Sh solution, which was stored at 4℃ until use. The CNF suspension (1.5% w/w) was sterilized at 121℃ for 15 min and also stored at 4℃ until use. The Sh solution and CNF suspension were mixed to obtain Sh:CNF (w/w) ratios of 100:0, 80:20, and 50:50 (total solid content = 2%, w/w), designated as CNF0, CNF20, and CNF50, respectively. Glycerol (0.6%, w/w) was added as a plasticizer to each mixture, followed by homogenization at 10,000 rpm for 3 min, stirring at 60℃ for 10 min, and cooling to room temperature prior to use. For film casting, 25 mL of each Sh-CNF mixture was poured into a polytetrafluoroethylene (PTFE)-coated Petri dish (12 cm inner diameter, SPL Life Sciences Co. Ltd., Pocheon, Korea) and oven-dried at 35℃ for 24 h. The resulting Sh-CNF composite films were peeled off from the dishes and conditioned in a desiccator containing saturated $Mg(NO_3)_2$ solution (53% RH, 25℃) for at least 48 h prior to analysis.

Aging of Sh-CNF composite films

The aging of Sh-CNF composite films was carried out according to the method by Soradech et al. (2013) with slight modifications. The films were placed in a desiccator containing saturated NaBr solution and stored at 40℃ and 53% RH for 7 days to induce aging,

under which significant changes in the properties of Sh film (CNF0) were observed.

Thickness measurements

Film thickness was measured using a digital micrometer (BD293-025, Bluetec, Shanghai, China). Six film specimens were prepared for each film type, and thickness was recorded at five different positions (center, top, bottom, left, and right) of each specimen. The mean thickness was calculated from a total of 30 individual measurements.

Opacity measurements

The opacity of the films was determined using a UV-Vis spectrophotometer (UV-1800, Shimadzu, Kyoto, Japan). Each film was cut into strips measuring 1×4 cm, and transmittance (T, %) was recorded at 600 nm. Opacity was then calculated according to equation (1) (Zhao et al., 2022; Kim et al., 2024).

$$Opacity = -\frac{\log T}{l} \quad (1)$$

where l=film thickness (μm). For each film type, four specimens were prepared, and opacity (mm^{-1}) was measured at five different positions per specimen. The mean value was calculated from a total of 20 measurements.

Moisture content measurements

The moisture content of the films was determined using a gravimetric method with slight modifications from the AOAC (2000) procedure. Film specimens were cut into squares (2×2 cm) and dried at 105℃ for 48 h. Moisture content was calculated from the mass difference before and after drying. Three specimens were analyzed for each film type, and the mean values were reported.

Water solubility measurements

The water solubility of the films was measured according to the method of Dordevic et al. (2023) with slight modifications. Film specimens were cut into squares (2×2 cm), dried at 105℃ for 24 h, and weighed to obtain the initial dry mass (M_1). The dried films were then immersed in 50 mL of distilled water at 25℃ for 24 h. The recovered films were dried again at 105℃ for 24 h and weighted to obtain the final dry mass (M_2). Water solubility was calculated using equation (2):

$$Water\ solubility\ (\%) = \frac{M_1 - M_2}{M_1} \times 100 \quad (2)$$

Three specimens were analyzed for each film type, and the mean values were reported.

Color measurements

The color of the films was measured using a colorimeter (CR-400, Konica Minolta, Osaka, Japan), calibrated against a standard white plate (L_0=94.69, a_0=4.56, b_0=−1.74). For each film type, five specimens were prepared, and the values of lightness (L^*), red-green coordinate (a^*), and yellow-blue coordinate (b^*) were recorded. The color difference (ΔE), whiteness index (WI), and yellowness index (YI) were calculated according to equations (3), (4), and (5), respectively (Ekrami et al., 2019).

$$\Delta E = \sqrt{(L^* - L_0)^2 + (a^* - a_0)^2 + (b^* - b_0)^2} \quad (3)$$

$$WI = 100 - \sqrt{(100 - L^*)^2 + a^{*2} + b^{*2}} \quad (4)$$

$$YI = 142.86\left(\frac{b^*}{L^*}\right) \quad (5)$$

Mechanical property measurements

The mechanical properties of the films were evaluated at 25℃ using a texture analyzer (TA1, Ametek Lloyd Instruments Ltd., Largo, FL, USA) following the methods of Lindström (2021) and Dai et al. (2017) with slight modifications. Film specimens were cut into strips (1×4 cm), and tensile tests were performed with an initial grip separation of 10 mm, a preload of 0.05 N, and a test speed of 3 mm/min to obtain stress–strain curves. Tensile strength (MPa) and elongation at break (%) were calculated according to equations (6) and (7).

$$Tensile\ strength = \frac{\tau}{A} \times 10^{-6} \quad (6)$$

$$Elongation\ at\ break = \frac{\Delta l}{l_0} \times 100 \quad (7)$$

where τ=stress at break (N), A=initial cross-sectional area of the film (m^2), Δl=elongation distance at break (mm), and l_0=initial grip separation distance (10 mm). Yield stress (MPa) was defined as the stress at the onset of strain increase in the stress-strain curve, while Young's modulus (MPa) was calculated as the slope of the initial linear region (strain<0.01). The work of break (MJ/m^3) was determined by integrating the area under the stress-strain curve up to the breaking point. For each film type, 15 specimens were tested, and mean values were reported.

Water vapor permeability measurements

The water vapor permeability (*WVP*) of the films was determined according to the ASTM E96 (ASTM, 2010) with slight modifications. Film specimens were cut into circular discs (7.5 cm diameter) and mounted over test cups (internal diameter=63.5 mm, internal height=50.8 mm) containing $CaCl_2$ to maintain 0% RH, with the edges sealed to prevent leakage. The cups were placed in a desiccator maintained at 53% RH using saturated $Mg(NO_3)_2$ solution and stored at 25℃ for 24 h. The cups were weighed at 3 h intervals. *WVP* ($g{\cdot}m/m^2{\cdot}day{\cdot}kPa$) was calculated using equation (8), based on Fick's first law:

$$WVP = \frac{l}{AP_{sat}\Delta RH}\frac{dm}{dt} \quad (8)$$

where l=film thickness (m), A=permeation area of the film (4.42×10^{-3} m^2), m=mass of cup (g), t=time (day), P_{sat}=saturation vapor pressure of water at 25℃ (3.17 kPa), and ΔRH=relative RH difference between the inside and outside of the cup (0.53). The change in cup mass over time in the steady-state region was analyzed by linear regression, and the resulting slop (dm/dt) was used for the calculation. For each film type, two specimens were tested, and mean values were reported.

Oxygen permeability measurements

The oxygen permeability (OP) of the films was determined according to ASTM D3985 (ASTM, 2002) using an oxygen permeation analyzer equipped with a coulometric sensor (M8101e, Systech Illinois, Oxfordshire, UK). Film specimens were mounted in the instrument with an effective test area (A) of 5×10^{-4} m^2. The RH in both the oxygen and nitrogen chambers were maintained at 0%, and the oxygen transmission rate ($\frac{l}{A}\frac{dV}{dt}$, $cm^3/m^2{\cdot}day$) was measured at 23℃ after reaching steady-state. *OP* ($cm^3{\cdot}m/m^2{\cdot}day{\cdot}atm$) was calculated based on Fick's first law using equation (9):

$$OP = \frac{l}{A\Delta P}\frac{dV}{dt} \quad (9)$$

where l=film thickness (m) and ΔP=oxygen partial pressure difference across the film (1 atm). For each film type, two specimens were analyzed, and mean values were reported.

Statistical analysis

All data were expressed as mean±standard deviation. Statistical analyses were performed using IBM SPSS Statistics software (version 26.0, IBM Co., Armonk, NY, USA). Differences among treatment groups were evaluated by one-way analysis of variance (ANOVA), and significant differences were identified using Duncan's multiple range test at a significance level of $p \leq 0.05$.

Results and Discussion

Effects of aging on thickness and opacity

The Sh film without CNF (CNF0) exhibited a thickness of 71 μm, which slightly decreased with increasing CNF content (Fig. 1). This reduction can be attributed to the denser film structure imparted by CNF, leading to lower moisture content (Kim et al., 2024). After the aging treatment, film thickness decreased further: CNF0 and CNF20 films showed only minor reductions of about 3–4%, whereas CNF50 film exhibited a significant decrease of 11.6% (Fig. 1). Since the films were aged at 40℃ and 53% RH for 7 days, the decrease cannot be ascribed to drying. In Sh-rich films (CNF0 and CNF20), self-polymerization or crosslinking among Sh molecules likely contracted the film network (Farag & Leopold, 2009; Coelho et al., 2012; Bar & Bianco-Peled, 2021; Chen et al., 2024). By contrast, the high CNF content in CNF50 film may have facilitated hydrogen bonding and structural rearrangement during aging, resulting in a more compact network and greater thickness reduction.

Film opacity increased 4.6-fold as the CNF ratio rose from 0% to 50% (Fig. 1), consistent with enhanced light scattering from the

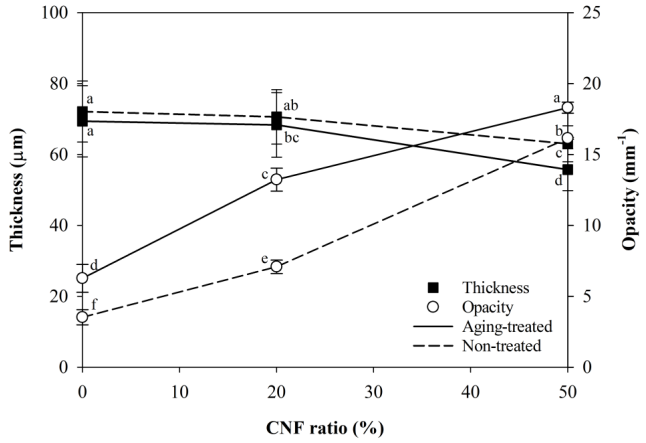

Fig. 1. Thickness and opacity of Sh-CNF composite films with and without aging treatment.

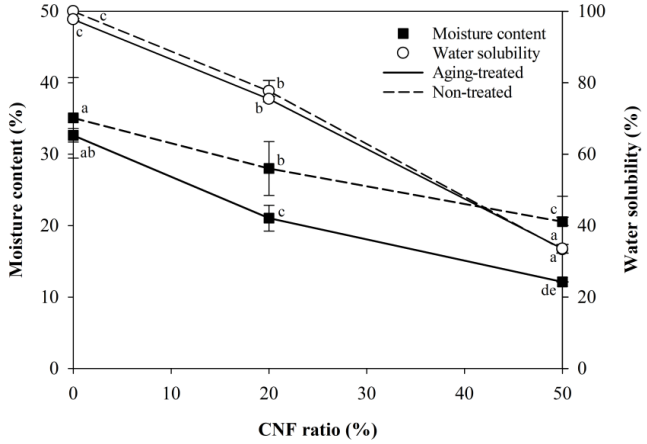

Fig. 2. Moisture content and water solubility of Sh-CNF composite films with and without aging treatment.

crystalline domains of CNF (Kim et al., 2024). The aging treatment further increased opacity. In CNF0 and CNF20 films, opacity nearly doubled, whereas the CNF 50 film, which already exhibited higher opacity due to the crystalline nature of CNF, showed only a moderate increase of 13.5% (Fig. 1). These changes suggest that crosslinking among Sh molecules during aging (Farag & Leopold, 2009; Coelho et al., 2012; Bar & Bianco-Peled, 2021; Chen et al., 2024), together with rearrangement of CNF molecules, produced a denser and more heterogeneous film network. Overall, the results demonstrate that aging treatment renders Sh-CNF films thinner and less transparent.

Effects of aging on moisture content and water solubility

As the CNF content increased from 0% to 50%, the moisture content of the films decreased from 35.1% to 20.6% (Fig. 2), which can be attributed to the denser film network formed by CNF (Kim et al., 2024). After aging treatment, the moisture content of all films significantly decreased. Specifically, the CNF0 film decreased from 35.1% to 32.6% (7% reduction), the CNF20 film from 28.0% to 21.1% (25% reduction), and the CNF50 film from 20.6% to 12.1% (41% reduction) (Fig. 2). The trend of greater moisture loss with higher CNF content was consistent with the thickness reduction results, suggesting that higher CNF levels promoted the formation of denser networks through structural rearrangement during aging. In Sh-rich films (CNF0 and CNF20), crosslinking among Sh molecules and the associated network contraction were likely the primary contributors to the reduced moisture content (Farag & Leopold, 2009; Coelho et al., 2012; Soradech et al., 2013; Bar & Bianco-Peled, 2021; Chen et al., 2024).

Film water solubility decreased sharply from 100% to 33.3% as the CNF content increased from 0% to 50% (Fig. 2), which is likely due to the denser hydrogen-bonded structure introduced by CNF (Kim et al., 2024). However, aging treatment did not cause any statistically significant changes in water solubility across all film types ($p \leq 0.05$) (Fig. 2). These findings indicate that although aging reduces the moisture content of the films by inducing Sh crosslinking and CNF rearrangement, the extent of network reorganization is insufficient to markedly affect water solubility.

Effects of aging on color

With increasing CNF content from 0% to 50%, the *WI* of the films decreased from 87.8 to 82.7, whereas the *YI* value increased from 11.5 to 20.8, indicating a reduction in whiteness and an enhancement of yellowish tones (Table 1). Concurrently, the *DE* value increased from 9.7 to 15.7, confirming a progressive deviation of the films from the white standard. These results suggest that the increase in crystalline domains and the formation of denser networks induced by CNF incorporation contributed to the yellowing of the films.

Following aging treatment, the CNF0 film, composed solely of Sh, exhibited pronounced color alterations. *DE* increased substantially from 9.7 to 17.2, *WI* decreased from 87.8 to 81.1, and *YI* rose sharply from 11.5 to 23.2 (Table 1). These findings indicate that aging treatment promoted yellowing of the films, which is consistent with

Table 1. Color difference (△*E*), whiteness index (*WI*), and yellowness index (*YI*) of Sh-CNF composite films with and without aging treatment

Films	Non-treated			Aging-treated		
	△*E*	*WI*	*YI*	△*E*	*WI*	*YI*
CNF0	9.7±1.7^{b}	87.8±1.6^{a}	11.5±2.5^{b}	17.2±1.0^{a}	81.1±0.8^{b}	23.2±1.7^{a}
CNF20	11.1±3.7^{b}	86.6±3.2^{a}	13.7±5.5^{b}	11.4±2.8^{b}	86.9±2.6^{a}	14.5±4.3^{b}
CNF50	15.7±1.5^{a}	82.7±1.4^{b}	20.8±2.3^{a}	16.7±0.6^{a}	83.1±1.4^{b}	21.9±0.9^{a}

previous reports attributing such changes to esterification and oxidation of Sh during storage, leading to the generation and modification of chromophores (Ciofini et al., 2016; Weththimuni et al., 2021). By contrast, the CNF20 film showed no significant changes in color parameters after aging and exhibited markedly lower color variation compared with the aged CNF0 film (Table 1). Similarly, the CNF50 film did not display significant color changes upon aging, and its color parameters remained comparable to those of the aged CNF0 film (Table 1). These results indicate that the incorporation of CNF effectively attenuated the yellowing reactions of Sh during storage.

Effects of aging on mechanical properties

As illustrated by the representative stress-strain curve (Fig. 3a), the mechanical properties of Sh-CNF composite films varied markedly with CNF content and aging treatment. As previously reported by Kim et al. (2024), increasing the CNF ratio from 0% to 50% resulted in higher tensile strength, yield stress, Young's modulus, and work of break, accompanied by a substantial decrease in elongation at break from 232% to 20% (Figs. 3b–f). These results reflect the role of CNF in reinforcing the film structure by forming a denser hydrogen-bonded network, thereby increasing stiffness and reducing flexibility (Kim et al., 2024).

After aging treatment, tensile strength, yield stress, Young's modulus, and work of break increased, whereas elongation at break decreased (Figs. 3b–f). These changes indicate that aging enhanced resistance to deformation. This effect is attributed to crosslinking and rearrangements among Sh molecules, as well as reorganization of CNF during aging, which together produced a more compact and rigid network (Farag & Leopold, 2009; Coelho et al., 2012; Bar & Bianco-Peled, 2021; Chen et al., 2024; Kim et al., 2024). The reduction in moisture content, which otherwise functions as a plasticizer, may have further contributed to the observed stiffening.

The extent of aging-induced changes in mechanical properties decreased with increasing CNF content. This suggests that CNF incorporation limited the progression of Sh crosslinking during

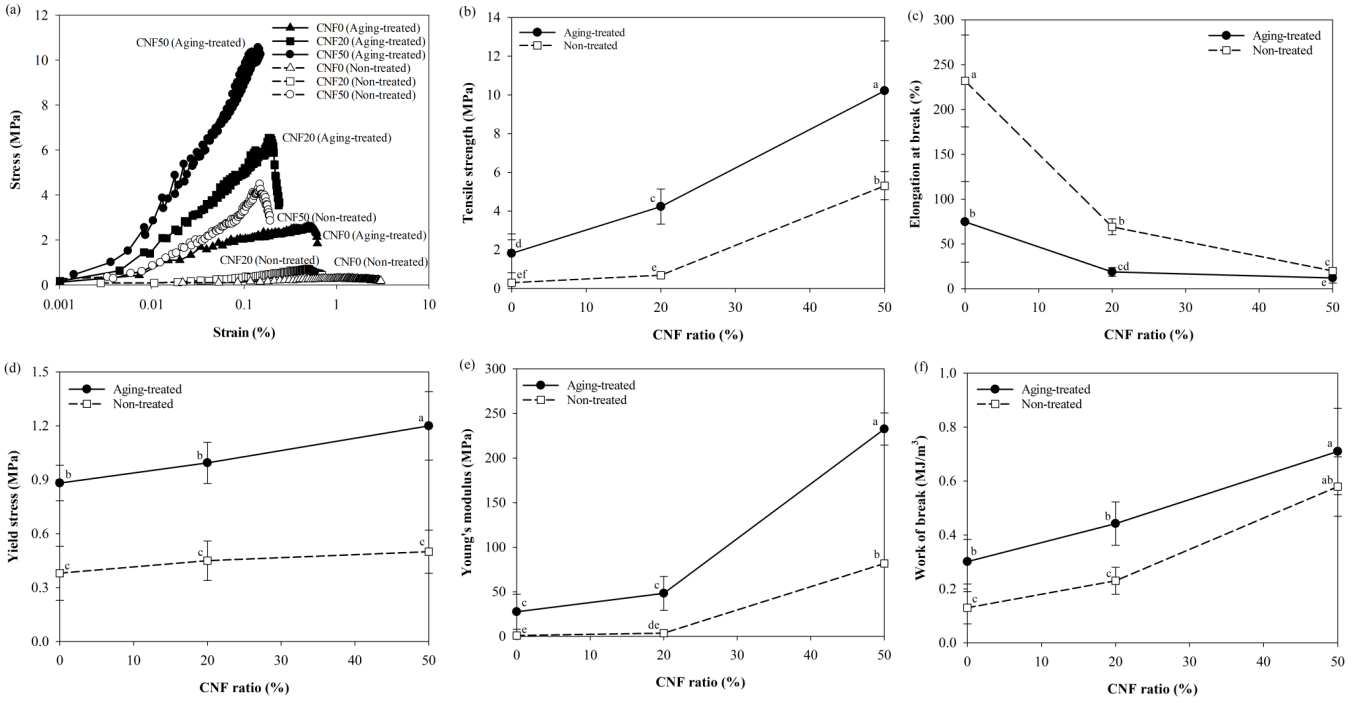

Fig. 3. Stress-strain curves (a), tensile strength (b), elongation at break (c), yield stress (d), Young's modulus (e), and work of break (f) of Sh-CNF composite films with and without aging treatment.

aging. Thus, while CNF addition strengthened and stiffened the films by restricting flexibility through network reinforcement, it simultaneously reduced the magnitude of property changes induced hy Sh aging.

Effects of aging on moisture and oxygen barrier properties

The CNF0 film, composed solely of Sh, exhibited a *WVP* of 5.7×10^{-4} g·m/m²·day·kPa. With increasing CNF content, *WVP* value increased markedly, reaching 1.1×10^{-3} g·m/m²·day·kPa in the CNF50 film, nearly double that of CNF0 (Fig. 4a). This trend indicates that CNF incorporation reduced the moisture barrier capacity of the films. In contrast, *OP* value decreased significantly

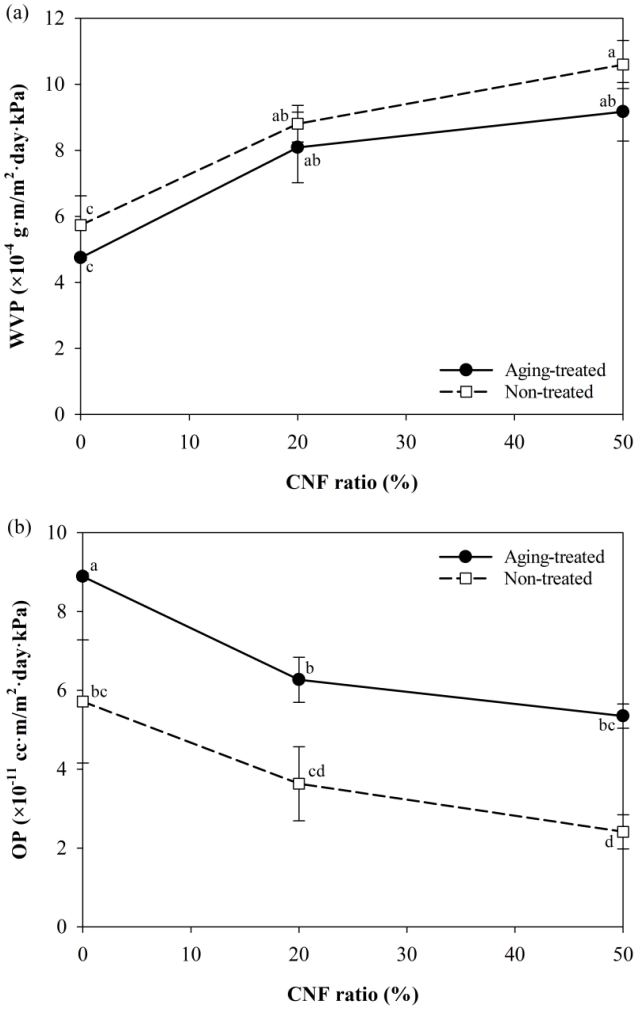

Fig. 4. Water vapor permeability (a) and oxygen permeability (b) of Sh-CNF composite films with and without aging treatment.

from 5.7×10^{-11} to 2.4×10^{-11} cc·m/m²·day·kPa (a 42% reduction) as CNF content increased from 0% to 50% (Fig. 4b), suggesting that CNF improved the oxygen barrier performance of the films.

Gas permeation through nonporous polymer films generally involves adsorption at the film surface with higher chemical potential, diffusion through the polymer matrix, and desorption at the opposite surface with lower chemical potential (Wang et al., 2018; Idris et al., 2022). In this study, CNF incorporation was shown to reduce film thickness, lower moisture content, and enhance mechanical strength. These changes can be attributed to the formation of a denser and stiffer network with reduced water-induced plasticization, thereby hindering gas permeation. In addition, CNF incorporation increased the fraction of crystalline regions impermeable to gas, thereby enhancing the tortuosity of the diffusion pathway, which further restricts gas permeation (Wang et al., 2018; Idris et al., 2022). The observed decrease in *OP* with increasing CNF content can thus be explained by these mechanisms. By contrast, the increase in *WVP* may be associated with water vapor transport through capillary channels in addition to diffusion. CNF incorporation could enhance film surface hydrophilicity, facilitating adsorption of water vapor (Wang et al., 2018; Kim et al., 2024). Adsorbed water molecules may expand the gaps between CNF fibrils, generating capillary networks that enable more rapid water transport (Wang et al., 2018).

Following aging treatment, *WVP* decreased by 83%–92% across all film types, while *OP* increased by 1.6-2.2-fold (Fig. 4). The reduction in *WVP* is consistent with crosslinking and rearrangement of Sh molecules, together with CNF reorganization, producing denser film networks with reduced free volume available for water vapor permeation (Luangtana-anan et al., 2007; Soradech et al., 2013). The increase in *OP* after aging was unexpected but may be explained by reduced hydrophilicity at the film surface and interior caused by molecular rearrangements during aging, which enhanced oxygen adsorption and diffusion to a greater extent than the barrier effect by free volume reduction.

Conclusion

This study demonstrated that aging markedly influenced the physicochemical, mechanical, and barrier properties of Sh-CNF composite films, depending on the blending ratio. Aging reduced film thickness, moisture content, and *WVP*, while enhancing tensile

strength, yield stress, Young's modulus, and work of break. These improvements are attributable to crosslinking of Sh through esterification and oxidation, together with CNF rearrangement via hydrogen bonding, which collectively produced denser and more rigid networks. At the same time, aging had unfavorable effects, including accelerated yellowing, reduced flexibility as indicated by decreased elongation at break, and diminishing oxygen barrier capacity. This study confirms that the properties of Sh-CNF films can be tuned not only by adjusting the Sh-to-CNF ratio but also through controlled aging. This complementary blending strategy between Sh and CNF, two biopolymers with contrasting film-forming characteristics, provides a promising approach for the design of edible films. Further studies should investigate a broader range of aging conditions (temperature, RH, and duration) to more precisely elucidate the application potential of Sh-CNF films.

ORCID

Hyo Jin Kim https://orcid.org/0000-0002-5757-8773
Donghwa Chung https://orcid.org/0000-0003-3397-5886

Conflict of interests

No potential conflict of interest relevant to this article was reported.

Acknowledgements

This work was supported by the Technology Innovation Program (or Industrial Strategic Technology Development Program) (20018683, Development of technology for manufacturing biomass-based cellulose fibers and commercializing edible coating) funded by the Ministry of Trade, Industry & Energy (MOTIE, Korea).

Data availability

Upon reasonable request, the datasets of this study can be available from the corresponding author.

Authorship contribution statement

Conceptualization: Chung D.
Data curation: Kim DH, Song Y, Chung H, Kim HJ, Chung D.
Formal analysis: Kim DH, Park G, Lee H.
Methodology: Kim DH, Park G, Lee H, Chung H, Chung D.
Software: Kim DH, Song Y.
Validation: Song Y, Chung H, Chung D.
Investigation: Kim DH.
Writing - original draft: Kim DH.
Writing - review & editing: Kim DH, Song Y, Park G, Lee H, Chung H, Kim HJ, Chung D.

Ethics approval

Not applicable.

References

Ahuja A, Rastogi VK. 2024. Physicochemical and thermal characterization of the edible shellac films incorporated with oleic acid to enhance flexibility, water barrier and retard aging. Int. J. Biol. Macromol. 269: 132136.

Alves L, Ferraz E, Gamelas JAF. 2019. Composites of nanofibrillated cellulose with clay minerals: a review. Adv. Colloid Interface Sci. 272: 101994.

AOAC. 2000. Official Method of Analysis of AOAC. 17 th ed. AOAC International, Rockville, MD, USA.

ASTM. 2002. Standard test method for oxygen gas transmission rate through plastic film and sheeting using a coulometric sensor (ASTM D3985-02). ASTM International, West Conshohocken, PA, USA.

ASTM. 2010. Standard test methods for water vapor transmission of materials (ASTM E96/E96M-10). ASTM International, West Conshohocken, PA, USA.

Bar H, Bianco-Peled H. 2021. The unique nanostructure of shellac films. Prog. Org. Coat. 157: 106328.

Basumatary IB, Mukherjee A, Katiyar V, Kumar S. 2022. Biopolymer-based nanocomposite films and coatings: recent advances in shelf-life improvement of fruits and vegetables. Critical reviews in food science and nutrition. Crit. Rev. Food Sci. Nutr. 62: 1912-1935.

Chen Y, Zhu Z, Shi K, Jiang Z, Guan C, Zhang L, Yang T, Xie F. 2024. Shellac-based materials: structures, properties, and applications. Int. J. Biol. Macromol. 279: 135102.

Ciofini D, Striova J, Camaiti M, Siano S. 2016. Photo-oxidative kinetics of solvent and oil-based terpenoid varnishes. Polym. Degrad. Stab. 123: 47-61.

Dai L, Long Z, Chen J, An X, Cheng D, Khan A, Ni, Y. 2017. Robust guar gum/cellulose nanofibrils multilayer films with good barrier properties. ACS Appl. Mater. Interfaces. 9: 5477-5485.

Dordevic D, Dordevic S, Abdullah FAA, Mader T, Medimorec

N, Tremlova B, Kushkevych I. 2023. Edible/biodegradable packaging with the addition of spent coffee grounds oil. Foods. 12: 2626.

Ekrami M, Emam-Djomeh Z, Ghoreishy SA, Najari Z, Shakoury N. 2019. Characterization of a high-performance edible film based on Salep mucilage functionalized with pennyroyal (*Mentha pulegium*). Int. J. Biol. Macromol. 133: 529-537.

Farag Y, Leopold CS. 2009. Physicochemical properties of various shellac types. Dissolut. Technol. 16: 33-39.

Guivier M, Chevigny C, Domenek S, Casalinho J, Perré P, Almeida G. 2024. Water vapor transport properties of bio-based multilayer materials determined by original and complementary methods. Sci. Rep. 14: 50.

Idris A, Muntean A, Mesic B. 2022. A review on predictive tortuosity models for composite films in gas barrier applications. J. Coat. Technol. Res. 19: 699-716.

Kim DH, Chung H, Kim HJ, Min WK, Chung D. 2024. Physicochemical and mechanical properties of cellulose nanofiber-shellac composite films. Food Eng. Prog. 28: 263-270.

Kumar S, Cherwoo L, Puri N, Sharma A, Thombare N, Bhondekar AP. 2023. Shellac: a natural lipid polymer for food safety and quality monitoring. In: Nanotechnology Applications for Food Safety and Quality Monitoring. Sharma A, Vijayakumar PS, Prabhakar EPK, Kumar R. (eds.). Academic Press, pp. 135-154.

Lindström T. 2021. A proposition for the estimation of the maximum tensile strength of variously charged nanocellulosic film materials provided by vacuum filtration. Nanomaterials. 11: 543.

Luangtana-anan M, Limmatvapirat S, Nunthanid J, Wanawongthai C, Chalongsuk R, Puttipipatkhachorn S. 2007. Effect of salts and plasticizers on stability of shellac film. J. Agric. Food Chem. 55: 687-692.

Pakharenko V, Sameni J, Konar S, Pervaiz M, Yang W, Tjong J, Oksman K, Sain M. 2021. Cellulose nanofiber thin-films as transparent and durable flexible substrates for electronic devices. Mater. Des. 197: 109274.

Pirozzi A, Ferrari G, Donsì F. 2021. The use of nanocellulose in edible coatings for the preservation of perishable fruits and vegetables. Coatings. 11: 990.

Poulose A, Parameswaranpillai J, George JJ, Gopi JA, Krishnasamy S, Dominic CDM, Hameed N, Salim NV, Radoor S, Sienkiewicz N. 2022. Nanocellulose: a fundamental material for science and technology applications. Molecules. 27: 8032.

Sharma A, Thakur M, Bhattacharya M, Mandal T, Goswami S. 2019. Commercial application of cellulose nano-composites: a review. Biotechnol. Rep. 21: e00316.

Soradech S, Limatvapirat S, Luangtana-anan M. 2013. Stability enhancement of shellac by formation of composite film: Effect of gelatin and plasticizers. J. Food Eng. 116: 572-580.

Thombare N, Kumar S' Kumari U, Sakare P, Yogi RK, Prasad N, Sharma KK. 2022. Shellac as a multifunctional biopolymer: a review on properties, applications and future potential. Int. J. Biol. Macromol. 215: 203-223.

Wang J, Gardner DJ, Stark NM, Bousfield DW, Tajvidi M, Cai Z. 2018. Moisture and oxygen barrier properties of cellulose nanomaterial-based films. ACS Sustain. Chem. Eng. 6: 49-70.

Wang J, Wang X, Liu B, Xiao J, Fang Z. 2025. Shellac-based films/coatings: Progress, applications and future trends in the field of food packaging. Food Chem. 467: 142326.

Weththimuni ML, Milanese C, Licchelli M, Malagodi M. 2021. Improving the protective properties of shellac-based varnishes by functionalized nanoparticles. Coatings. 11: 419.

Yu Z, Alsammarraie FK, Nayigiziki FX, Wang W, Vardhanabhuti B, Mustapha A, Lin M. 2017. Effect and mechanism of cellulose nanofibrils on the active functions of biopolymer-based nano-composite films. Food Res. Int. 99: 166-172.

Yuan Y, He N, Xue Q, Guo Q, Dong L, Haruna MH, Zhang, Xia, Li B, Li L. 2021. Shellac: a promising natural polymer in the food industry. Trends Food Sci. Tech. 109: 139-153.

Zhao J, Wang Y, Liu C. 2022. Film transparency and opacity measurements. Food Anal. Methods. 15: 2840-2846.size distribution and composition in dark chocolate. Int. J. Food Sci. Technol. 44: 111-119.